

Design of Tilted-Beam Fabry-Perot Antenna with Aperiodic Partially Reflective Surface

You-Feng Cheng, Wei Shao, Xiao Ding, and Meng-Xia Yu

School of Physical Electronics

University of Electronic Science and Technology of China, Chengdu, 610054, China
juvengcheng1377@gmail.com, weishao@uestc.edu.cn, xding@uestc.edu.cn, yumengxia@263.net

Abstract — A fast synthesis model for designing high-gain tilted-beam antennas with the aperiodic partially reflective surface (PRS) is presented in this paper. In this model, concepts of array synthesis and thinning are introduced to realize the tilted beam and control the sidelobe level (SLL). Since a large number of data need to be processed during the optimization process, an efficient hybrid real-binary bat algorithm (HRBBA) is proposed and embedded in the model to optimize the loop widths and the absence of the square loops on the PRS. As an example, an antenna with an expected tilted beam in the elevation plane ($\theta = 40^\circ$) is manufactured and measured, and both the simulated and measured results show that the antenna can tilt its beam toward the expected direction with good performance.

Index Terms — Big data, Fabry-Perot (FP) antenna, Hybrid Real-Binary Bat Algorithm (HRBBA), Partially Reflective Surface (PRS), tilted-beam antenna.

I. INTRODUCTION

Tilted-beam antennas are widely used in modern communication systems, such as in satellite communication systems, wireless LAN (WLAN) systems and mobile communication systems [1]. A common approach to achieve high gain and titled beam is the phased array. However, due to the complex feed system and limited space, the phased array is not suitable for some applications. In the literature, several single element antennas have been proposed with good performance. In [2-5], spiral antennas with tilted beams are analyzed and investigated. These antennas possess asymmetric off-broadside beams in the elevation plane. In [6], a printed star antenna which can generate both doughnut-shaped and tilted beam radiation patterns is presented, and its tilted beam depends on the star flare angle. [7] and [8] present two circularly polarized tilted-beam antennas whose radiation patterns possess a beam pointing angle at 30° and 50° , respectively.

A partially reflective surface (PRS) placed in front of a patch antenna can increase its gain due to the

multiple reflections of electromagnetic waves between the two planes [9-11]. Furthermore, this structure possesses a potential to tilt the radiation beam. [12] proposes an antenna system composed of a patch antenna and arrayed loops. The loops are periodically placed on the parasitic substrate which makes the antenna system radiate a tilted high-gain beam. However, there is a lack of fast synthesis model for forming the tilted beam. In [13], a reconfigurable PRS is used for beam steering with the help of RF micro electro-mechanical system (MEMS) switches. The high-gain antenna can control the beam shape among broadside, symmetric conical, and an asymmetric single beam which is either frequency-scanned or steered at the fixed frequency.

This paper presents an efficient design method for the high-gain tilted-beam antenna from the perspective of array synthesis and thinning. Initially, 7×7 uniform square strip loops are applied to obtain good resonant characteristics at a fixed frequency of 5.2 GHz. Then, by means of a fast synthesis model, the phase distribution of the electric field over the PRS is changed by optimizing the loop widths, and the radiation pattern is tilted toward an arbitrary expected direction in the elevation plane. This operation not only provides the tilted-beam design, but also increases the design freedom. At last, the concept of array thinning is introduced into the design. Several loops are removed for the purpose of sidelobe level (SLL) reduction. An improved hybrid real-binary bat algorithm (HRBBA) is applied to the optimization of the aperiodic PRS due to the generated big data. As an example, an antenna with an expected tilted beam ($\theta = 40^\circ$) is manufactured and measured, and both the simulated and measured results show that the proposed antenna can tilt the maximum beam in the elevation plane with good performance.

II. FAST SYNTHESIS MODEL

A fast synthesis model is proposed for forming the tilted beam. The flowchart of the fast synthesis model is shown in Fig. 1. There are two interrelated modules in this model, namely the optimization module and the

simulation module, respectively.

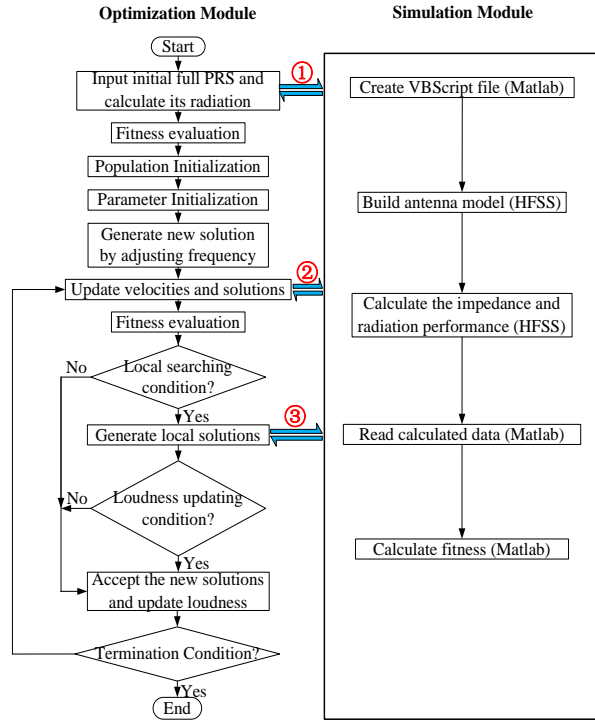


Fig. 1. Flowchart of the fast synthesis model for forming the tilted beam.

Initially, a full PRS (as shown in Fig. 2 (c)) with uniform loop widths, which radiates a high-gain broadside beam, is adopted for the antenna design. Then for the purpose of steering the radiation beam toward any expected directions in the elevation plane, the loop widths and the absence of the square loops should be optimized in the optimization module. As an efficient meta-heuristic method, here the bat algorithm (BA) is selected as a useful tool for the optimization problem. In each generation, for fast and accurate numerical analysis of each newly generated PRS, the BA programed in the Matlab software is linked with a full-wave solver based on the ANSYS High Frequency Structure Simulator (HFSS) in the simulation module. The link between Matlab and HFSS is realized through the macro programming. Matlab inputs the optimization parameters and calls HFSS to simulate the reflection coefficient and far-field pattern of the proposed antenna. Next, the simulated results from HFSS are returned to Matlab and used to calculate the cost functions. After a few generations, a thinned PRS with optimized loop widths is obtained and used for the final tilted-beam antenna design. Note that only the three steps marked with arrows and circled numbers in the Optimization Module are linked to the Simulation Module.

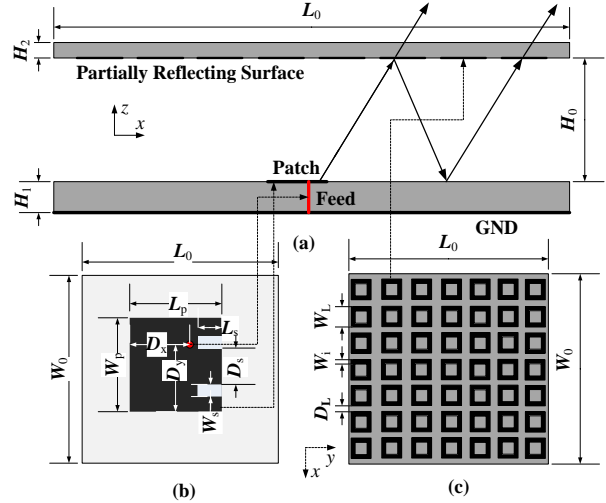


Fig. 2. Initial structure of the proposed antenna. (a) Side view, (b) source antenna, and (c) PRS.

Besides the beam tilt, resonant frequency and gain, the sidelobe level (SLL), which maybe deteriorates in the optimization, is another important objective for the antenna design. Therefore, the objective functions are given as below:

$$objv_1 = \begin{cases} 0 & \text{if } S_{11}(f_0) < -10 \text{ dB} \\ 1 & \text{if } S_{11}(f_0) \geq -10 \text{ dB} \end{cases}, \quad (1)$$

$$objv_2 = Gain, \quad objv_3 = SLL, \quad objv_4 = |\theta_t - \theta_0|,$$

where f_0 is the expected resonant frequency, namely 5.2 GHz in this paper, $Gain$ is the realized gain, SLL is the peak sidelobe level, θ_0 is the expected tilted direction and θ_t is the direction corresponding to the maximum value of the pattern in the xoz plane. Here $Objv_1$ represents the resonance characteristics of the antenna, $Objv_2$ and $Objv_3$ yield a high gain and a low SLL, and $Objv_4$ makes the maximum beam tilt to an expected direction. Thus, the fitness function of the optimization problem can be written as:

$$Fitness = \omega_1 \cdot Objv_1 + \omega_2 \cdot Objv_2 + \omega_3 \cdot Objv_3 + \omega_4 \cdot Objv_4, \quad (2)$$

where ω_1 , ω_2 , ω_3 and ω_4 are weight values, and they are selected as 0.2, 0.2, 0.2 and 0.4, respectively. It is worth noting that θ_0 determines the beam tilting of the design, which increases the design freedom greatly.

III. ANTENNA DESIGN

A. Initial structure and its analysis

The initial structure with uniform square strip loops placed on a parasitic substrate is shown in Fig. 2. An E-shaped patch with increased bandwidth is fabricated on the bottom substrate as the radiation source [14]. The grounded FR4 substrate has a thickness of 3.2 mm and a

relative permittivity of 4.4. A coaxial probe penetrates the bottom substrate to provide the excitation for the square patch. On the parasitic substrate, the 7×7 uniform square strip loops are periodically arranged to constitute the PRS. The parasitic substrate is Rogers 5880 with a relative permittivity of 2.2 and a thickness of 0.508 mm. The distance H_0 between the source antenna and the PRS is about half wavelength. The antenna operates at 5.2 GHz with a total size of $154 \text{ mm} \times 154 \text{ mm} \times 30.4 \text{ mm}$.

The detail physical parameters of the proposed antenna are: $L_0 = W_0 = 35 \text{ mm}$, $L_p = 15.2 \text{ mm}$, $L_s = 3 \text{ mm}$, $W_s = 1.7 \text{ mm}$, $W_L = 18.5 \text{ mm}$, $D_L = 3.5 \text{ mm}$, $D_x = 10.2 \text{ mm}$, $D_y = 10.4 \text{ mm}$, $D_s = 4 \text{ mm}$, $H_0 = 28.9 \text{ mm}$, $H_1 = 3.2 \text{ mm}$ and $H_2 = 0.508 \text{ mm}$. All these parameters are fixed throughout this paper except the width of each loop W_i ($i = 1, 2, \dots, 7$) which is set as 2.5 mm initially and will be optimized in the fast synthesis model.

A Fabry-Perot (FP) cavity is formed by the PEC ground plane and the PRS, and the multiple transmission and reflection of the electromagnetic waves generated by the radiation source occur inside the cavity. Thus, the initial antenna would radiate a high-gain broadside beam. Here a scalar-based analysis for the antenna is formulated. Note that the weak mutual coupling effects among the loops are ignored in the analysis.

Assuming the far-field electric field of the source antenna is $E_{\text{source}}(r, \theta, \phi)$, the total radiated power of the source antenna in the upper half space can be calculated as:

$$P_{\text{source}} = \frac{1}{2\eta_0} \int_0^{2\pi} \int_0^{\pi/2} |E_{\text{source}}(r, \theta, \phi)|^2 r^2 \sin\theta d\theta d\phi, \quad (3)$$

where η_0 is the free-space impedance.

In terms of the loop m of the PRS, the power flow density of the incident plane wave from the source antenna and towards the direction of the loop is:

$$S(r^m, \theta^m, \phi^m) = \frac{|E_{\text{source}}(r^m, \theta^m, \phi^m)|^2}{2\eta_0}, \quad (4)$$

where (r^m, θ^m, ϕ^m) is the loop position. Then the available power of each loop can be written in terms of the power flow density and the effective area (A_e) of the loop, and that is:

$$P_c^m = S(r^m, \theta^m, \phi^m) A_e \cos \delta^m, \quad (5)$$

where δ^m is the angle between the radial vector of the incident power flow density and the unit vector normal to the loop m . According to the transmission coefficient of the loop, the transmitted power of the loop can be given by:

$$P_t^m = P_c^m |S_{21}^m|^2. \quad (6)$$

Therefore, the transmitted electric field (E^m) of loop m can be obtained:

$$E^m(r, \theta, \phi) = \sqrt{\frac{2\eta_0 P_t^m D_{\text{Loop}}(\theta, \phi)}{4\pi r^2}} e^{j(-kr^m + k\hat{r} \cdot \mathbf{r}^m + \gamma^m)}, \quad (7)$$

where $D_{\text{Loop}}(\theta, \phi) = G_{\text{Loop}}(\theta, \phi)/\varepsilon_{\text{rad}}$, ε_{rad} is the radiation efficiency, $G_{\text{Loop}}(\theta, \phi) = (\frac{4\pi}{\lambda_0^2}) A_e$, λ_0 is the free-space wavelength and γ^m is a phase term determined by the loop. It can be seen from (5)-(7) that the far-field electric field of the PRS is dependent on A_e , $|S_{21}|$, γ^m and the loop position. Moreover, A_e and $|S_{21}|$ determine the far-field amplitude, and γ^m and the loop position determine the phase.

At last, the far-field electric field of the PRS in the upper half space can be calculated as the superposition of the fields of all loops, and it can be expressed as:

$$E_{\text{PRS}} = \sum_{m=1}^M E_m(r, \theta, \phi) e^{-jkr}. \quad (8)$$

B. Tilted-beam realization

Equation (8) represents the far-field electric field of an FP antenna relating to the PRS elements. Note that (8) is similar to the formula of the array factor of a phased array in form. In addition, when the loop width is changed, A_e , $|S_{21}|$ and γ^m of the loop would all be changed but the loop position is fixed. It means that the loop widths determine the amplitudes and phases of the PRS elements. That is to say, by optimizing the loop widths, array synthesis techniques can be used for forming the tilted beam in the design. Unfortunately, accurate calculation of (8) is hard to be realized due to the uncertainty of E_{source} . Thus, the far-field and input characteristics with different PRS are obtained by the HFSS simulations.

However, one of the problems that may arise in the optimization is the deterioration of the SLL. In order to realize the low sidelobe, the concept of array thinning is introduced into the optimization since one advantage of array thinning is that lower sidelobes can be obtained [15-17]. A thinned PRS with some square loops removed has the capability to reduce the SLL of the optimized antenna. In addition, the thinned PRS increases the gain due to the sidelobe suppression.

The PRS characterized by rectangular unit cells with serial numbers is illustrated in Fig. 3. In order to generate expected tilted beams in the xoz plane with good performance, loop widths in each row are fixed to be the same, and those in each column ($W_1 - W_7$) are optimized in a range from 0.25 mm to 6.25 mm. Furthermore, PRS loops, which are listed from 0 to 49 in Fig. 3, are determined to be retained or removed in the optimization. Thus in the whole synthesis, there are 56 optimization variables (7 real variables and 49 binary ones), and the optimization objectives are expressed in (1).

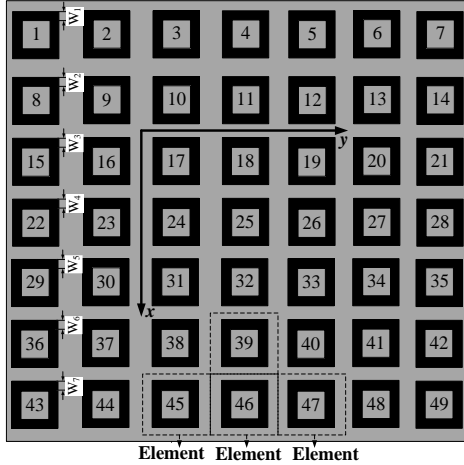


Fig. 3. PRS characterized by rectangular unit cells with serial numbers.

IV. IMPROVED HRBBA

In order to optimize the loop widths and the absence of the square loops, the multi-objective BA [18-20], which can efficiently and reliably process big-data optimization problems, is selected as the synthesis algorithm. Inspired from the echolocation of micro bats, BA has shown that it is very promising and could outperform most existing algorithms.

The basic BA can be briefly described as follows. There are five characteristic parameters in the algorithm: the frequency f , the velocity v , the position x , the loudness A and the rate of pulse emission r . For each bat (i), its frequency f_i , position x_i and velocity v_i are updated by:

$$f_i = f_{\min} + \beta(f_{\max} - f_{\min}), \quad (9)$$

$$v_i' = v_i^{t-1} + (x_i^{t-1} - x^*)f_i, \quad (10)$$

$$x_i' = x_i^{t-1} + v_i', \quad (11)$$

where t represents the time step. β is a random vector drawn from a uniform distribution and it is in the range of $[0, 1]$. $[f_{\min}, f_{\max}]$ is the range of the frequency, and it is set as $[0, 100]$ in this problem. Initially, each bat is randomly assigned a frequency that is drawn uniformly from $[f_{\min}, f_{\max}]$. x^* is the current global best solution. In terms of the local search part, when a solution is selected among the current best solutions, a local random walk is used for each bat to generate a new solution, and it can be calculated by:

$$x_{\text{new}} = x_{\text{old}} + \varepsilon A^t, \quad (12)$$

where ε is a random number drawn from $[-1, 1]$. And the loudness is updated by:

$$A_i^{t+1} = \alpha A_i^t, \quad r_i^{t+1} = r_i^0 (1 - e^{-\gamma}), \quad (13)$$

where α and γ are constants, and they are set as $\alpha = \gamma = 0.9$ in this problem. It can be seen that, compared with

other algorithms, the algorithm uses the frequency-based tuning and pulse emission rate to mimic bat behaviors, and this leads to a good convergence and simple implementation. Furthermore, the authors in [14] use a weighted sum to combine multi objectives into a single objective.

In the antenna design, the parameter vector of each solution consists of 56 variables: $x = [W_1, W_2, \dots, W_7, LA_1, LA_2, \dots, LA_{49}]$. Here LA_n represents the presence or absence of the n th loop shown in Fig. 3. When there is a square loop in the position, LA_n is set as 1, and it is set as 0 when there is no loop in this position. It is worth noting that W_n and LA_n are of different types. W_n is a continuous variable while LA_n is a discrete one which only can be 0 or 1. The traditional real-number BA is incapable of solving this problem. On the other hand, since the binary coding of the real variables has more dimensions than the real one, the binary algorithms, such as genetic algorithm, are inefficient for the optimization compared to a hybrid-parameter algorithm [21]. An improved HRBBA is proposed here for this case.

The improved HRBBA is divided into two parts, namely the real part and the binary one. Each individual is represented by an $(N_r + N_b)$ -dimensional vector:

$$\vec{x} = \{x_r^1, x_r^2, \dots, x_r^{N_r}, x_b^1, x_b^2, \dots, x_b^{N_b}\}. \quad (14)$$

At each generation, the real and binary parts share the same characteristic parameters and global best solutions. In the real part, the algorithm process is the same as the basic BA. While in the binary part, updated parameters, such as v and x , may be fallen outside their range $[0, 1]$. To make the parameters update in an alternative manner, the sigmoid limiting transformation is implemented in the algorithm by defining an intermediate variable [22]:

$$S(v^m) = \frac{1}{1 + e^{-v^m}}. \quad (15)$$

The binary BA can be described as follows. Firstly, parameters v and x are initialized as binary-valued ones. Then parameters f and v are also updated by the formulations in (9) and (11). Note that v is limited in a range of $[-V_{\max}, V_{\max}]$ and V_{\max} is selected as 6 in the proposed design. $S(x)$ can be calculated by (15) and its range is $[1/(1+e^{V_{\max}}), 1/(1+e^{-V_{\max}})]$. The value of $S(v^m)$ represents a probability threshold, and then x can be updated by:

$$x_b^m = \begin{cases} 1, & \text{if } r^m < S(v^m) \\ 0, & \text{if } r^m \geq S(v^m) \end{cases}, \quad (16)$$

where r^m is a random number with a uniform distribution in the range of $[0, 1]$. From (16), it can be indicated that the probability that the m th bit equals to 1 is $S(v^m)$.

In each generation of the improved HRBBA, after the independent completion of the real and binary parts, the fitness functions can be calculated based on the newly-generated individuals.

Finally, in this design, the HRBBA is embedded into the synthesis as shown in Fig. 1.

In order to verify the optimization performance of the proposed HRBBA, the classic functional testbeds are shown here by using the Rastrigin fitness function:

$$f(x) = \sum_{i=1}^3 [x_i^2 - 10 \cos(2\pi x_i) + 10], \quad (17)$$

where x_1 and x_2 are real variables in a range of $[-5, 5]$, x_3 is related to the 16-bit binary part via a binary-to-real mapping:

$$x_3 = \frac{10}{2^{16} - 1} \sum_{N=1}^{16} 2^{N-1} \cdot B_N - 5, \quad (18)$$

and B_N is 0 or 1. Thus the total 18-dimensional solution space is composed of two real variables and sixteen binary bits.

The traditional GA, binary particle swarm optimization (BPSO) and hybrid real-binary PSO (HPSO) algorithms presented in [22] are used here to illustrate the superiority of the proposed HRBBA. For GA, the recombination probability is chosen as 0.7. For BPSO and HPSO, the acceleration coefficients c_1 and c_2 are both chosen as 2. The velocities in the real part of HPSO and HRBBA are distributed in a range of $[-0.5, 0.5]$, and the maximum velocities in the binary part of BPSO, HPSO and HRBBA are all chosen as 6. In addition, in HRBBA, the loudness and pulse emission control parameters (α and γ) are selected as 0.95 and 0.95, respectively.

In the optimization, a population with 10 individuals is used for 200 iterations. In Table 1, the minimum, maximum and mean values of the fitness from the 200 executions of GA, BPSO, HPSO and HRBBA are presented. It can be seen that hybrid real-binary algorithms (HPSO and HRBBA) is able to find lower fitness values than the binary algorithms (GA and BPSO), which means the hybrid real-binary algorithms have a more powerful optimizing ability. Moreover, the obtained maximum and mean fitness values of HRBBA are lower than those of HPSO, which means HRBBA is better than HPSO for optimizing such a single-objective function, although the minimum fitness value of HRBBA is a litter higher than that of HPSO. To reflect the convergence characteristics of the algorithms, Fig. 4 shows the best fitness values at each iteration over 200 trials. Obviously, HRBBA has the fastest convergence speed.

Table 1: Final optimized results derived from GA, BPSO, HPSO and HRBBA after 200 executions

	Maximum	Minimum	Mean
GA	11.94	1.06×10^{-5}	3.72
BPSO	8.95	3.46×10^{-6}	3.65
HPSO	0.39	8.52×10^{-6}	1.77×10^{-2}
HRBBA	4.97×10^{-2}	4.75×10^{-5}	1.31×10^{-2}

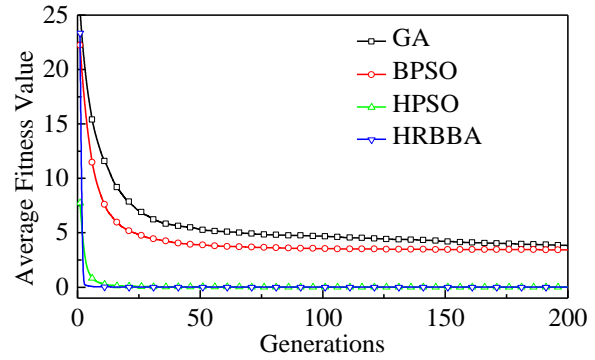


Fig. 4. Comparison of best values averaged over 200 trials for GA, BPSO, HPSO and HRBBA.

V. EXPERIMENT VALIDATION

Here, a design of an antenna with radiation beam toward $\theta = 40^\circ$ is shown to validate the proposed design method. The optimized PRS of the antenna is shown in Table 2, where “1” indicates that the square loop arranged with serial number in Fig. 3 is retained while “0” indicates that the square loop is removed. The optimized FP antenna with aperiodic PRS is fabricated and measured. The prototype of the antenna and the PRS are shown in Fig. 5.

Table 2: Optimized aperiodic PRS (unit: mm)

Widths	W_1	W_2	W_3	W_4	W_5	W_6	W_7
	0.40	4.10	2.60	1.45	0.55	0.70	0
Distribution	1111011001101011111010110110111111 11010001000000						

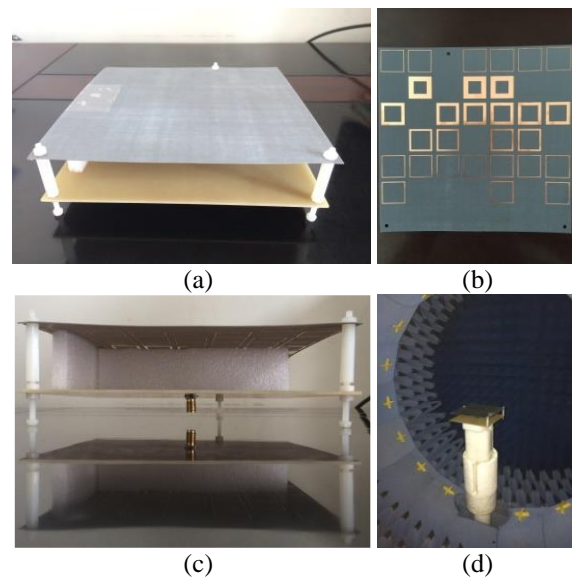


Fig. 5. Photographs of the prototype of the proposed FP antenna. (a) 3D view, (b) aperiodic PRS, (c) front view, and (d) masurement in a Satimo Starlab nearfield measurement system.

The simulated and measured input performance in terms of S_{11} is depicted in Fig. 6. It can be seen that the proposed antenna possesses a bandwidth of 5.09-5.57 GHz with S_{11} lower than -10 dB from the measured results. The relative bandwidth of the proposed antenna is about 10%. Such a wide bandwidth is mainly due to the contribution of the structure of the source antenna. It is noted that the effect of the thinned PRS on the resonance characteristics is very small.

Figure 7 shows the simulated and measured radiation patterns. It can be seen that good agreement is found between the simulated and the measured results. The main lobe points to $\theta = 40^\circ$ in the elevation plane at 5.2 GHz. The measured SLL is -10.33 dB which is a litter higher than the simulated one. This mainly because the upper substrate is very soft and its surface is uneven.

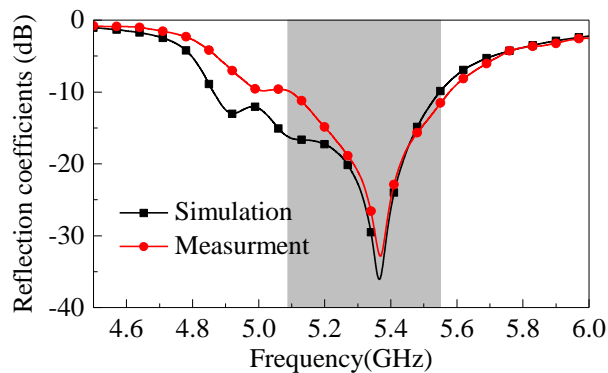


Fig. 6. Measured and simulated reflection coefficients of the optimized FP antenna.

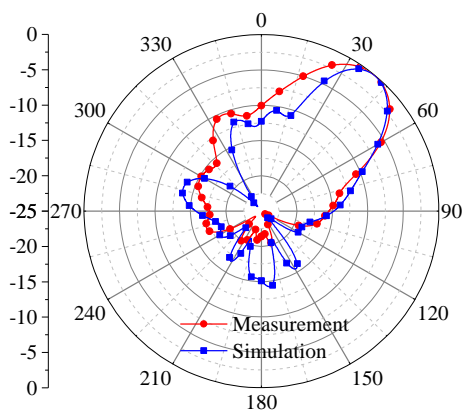


Fig. 7. Measured and simulated radiation patterns of the optimized antenna at 5.2 GHz in the xoz plane.

Figure 8 shows the measured peak gain and efficiency of the antenna. The peak gain at 5.2 GHz is 12.50 dBi, which is lower than the simulated one about 1 dB. This is mainly due to the loss of the measurement setup. The peak gain is about 11.12-13.45 dBi in the

bandwidth and the maximum gain appears at 5.45 GHz. It is worth noting that the PRS with more square loops can lead to a higher gain. The efficiency of the antenna mainly varies between 50% and 67%. At 5.2 GHz, the efficiency is 62%. The thinned PRS maybe decreases the efficiency of the antenna.

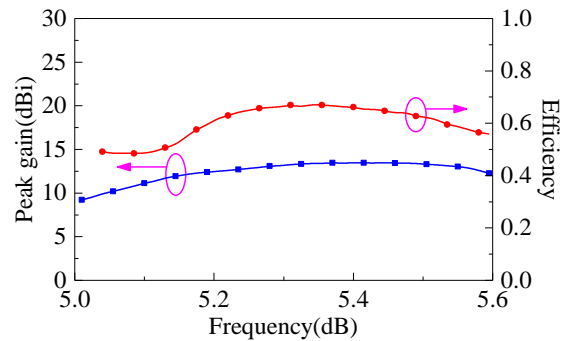


Fig. 8. Measured peak gain and efficiency of the optimized antenna.

At last, a comparison between the proposed design and that in [12] is given in Table 3. The antenna design method, PRS structure, design freedom and antenna performance are listed. An efficient fast synthesis model, which is lacked in [12], is proposed to design the antenna in our design. Based on the fast synthesis model, any required tilted radiation beams can be obtained by optimizing the PRS. In [12], only the antennas with some designated tilted beams can be designed with good performance. With the help of the synthesis model and the improved HRBBA, the aperiodic PRS structures, which afford benefit for the antenna radiation performance, are introduced in the proposed design. The periodic PRS structure restricts the tilted angle in [12.] In addition, the proposed design leads to a wider bandwidth due to the used source antenna, and the antennas designed in [12] have higher realized gains since PRSs with larger size are utilized. Overall, compared with the design method in [12], the proposed design possesses a higher design freedom and design convenience with the powerful synthesis model and the aperiodic PRS structure.

Table 3: Comparison of the antenna design between the proposed method and reference [12]

	Proposed Method	Ref. [12]
Fast synthesis model	Yes	No
Design freedom	Any required tilted beams	Some designated tilted beams
PRS structure	Aperiodic	Periodic
Antenna performance	Wider bandwidth	Higher gain

VI. CONCLUSION

In this paper, an efficient fast synthesis model is proposed to design a high-gain tilted-beam FP antenna with the aperiodic PRS. The FP antenna is analyzed and the concepts of array synthesis and thinning are introduced into the presented model. In addition, an improved HRBBA is proposed to optimize the loop widths and the absence of the square loops on the PRS. Experiment validation with an expected tilted beam ($\theta = 40^\circ$) shows the good performance and powerful design flexibility of the method.

ACKNOWLEDGMENT

This work was supported by the National Natural Science Foundation of China (No. 61471105 and 61401065) and the 973 Project of China (No. 613273).

REFERENCES

- [1] M. Arrebola, E. Carrasco, and J. A. Encinar, "Beam scanning antenna using a reflectarray as sub-reflector," *Applied Computational Electromagnetics Society Journal*, vol. 26, pp. 473-483, 2011.
- [2] H. Nakano, Y. Shinma, and J. Yamauchi, "A monofilar spiral antenna and its array above a ground plane—Formation of a circularly polarized tilted fan beam," *IEEE Trans. Antennas Propagat.*, vol. 45, pp. 1506-1511, Oct. 1997.
- [3] H. Nakano, J. Eto, Y. Okabe, and J. Yamauchi, "Tilted- and axial-beam formation by a single-arm rectangular spiral antenna with compact dielectric substrate and conducting plane," *IEEE Trans. Antennas Propagat.*, vol. 50, no. 1, pp. 17-24, Jan. 2002.
- [4] H. Nakano, Y. Okabe, H. Mimaki, and J. Yamauchi, "Monofilar spiral antenna excited through a helical wire," *IEEE Trans. Antennas Propagat.*, vol. 51, no. 3, pp. 661-664, Mar. 2003.
- [5] H. Nakano, N. Aso, N. Mizobe, and J. Yamauchi, "Low-profile composite helical-spiral antenna for a circularly-polarized tilted beam," *IEEE Trans. Antennas Propagat.*, vol. 59, pp. 2710-2713, July 2011.
- [6] A. Pal, A. Mehta, D. Mirshekar, and P. J. Messy, "Doughnut and tilted beam generation using a single star patch antenna," *IEEE Trans. Antennas Propagat.*, vol. 57, no. 10, pp. 3413-3418, Oct. 2009.
- [7] P. Ravindranath, S. Raghavan, and P. H. Rao, "Circularly polarized tilted beam microstrip antenna," *Computing Communication & Networking Technologies (ICCCNT), 2012 Third International Conference*, pp. 26-28, July 2012.
- [8] M. Lakshmi, A. Ambika, and P. H. Rao, "Circularly polarized tilted beam monopole antenna," *Communications and Signal Processing (ICCSP), 2014 International Conference*, pp. 973-976, Apr. 2014.
- [9] A. P. Feresidis and J. C. Vardaxoglou, "High gain planar antenna using optimized partially reflective surfaces," *Proc. Inst. Elect. Eng. Microwave Antennas Propagat.*, vol. 148, pp. 345-350, Dec. 2001.
- [10] F. Costa, A. Monorchio, and G. Manara "An overview of equivalent circuit modeling techniques of frequency selective surfaces and metasurfaces," *Applied Computational Electromagnetics Society Journal*, vol. 29, no. 12, pp. 960-976, Dec. 2014.
- [11] A. Pirhadi, H. Bahrami, and A. Mallahzadeh, "Electromagnetic band gap (EBG) superstrate resonator antenna design for monopulse radiation pattern," *Applied Computational Electromagnetics Society Journal*, vol. 27, no. 11, pp. 908-917, Nov. 2014.
- [12] H. Nakano, S. Mitsui, and J. Yamauchi, "Tilted-beam high gain antenna system composed of a patch antenna and periodically arrayed loops," *IEEE Trans. Antennas Propagat.*, vol. 62, no. 6, pp. 2917-2925, June 2014.
- [13] H. Moghadas, M. Daneshmand, and P. Mousavi, "MEMS-tunable half phase gradient partially reflective surface for beam-shaping," *IEEE Trans. Antennas Propagat.*, vol. 63, no. 1, pp. 369-373, Jan. 2015.
- [14] A. A. Razzaqi, M. Mustaqim, and B. A. Khawaja, "Wideband E-shaped antenna design for WLA applications," *2013 IEEE 9th Int. Conf. on Emerging Technologies (ICET)*, pp. 1-6, Dec. 2013.
- [15] R. L. Haupt, "Adaptive arrays," *Applied Computational Electromagnetics Society Journal*, 1983.
- [16] R. L. Haupt, "Thinned interleaved linear arrays," *ACES International Conference on Wireless Communications and Applied Computational Electromagnetics*, vol. 53, pp. 2858-2864, Sep. 2005.
- [17] R. L. Haupt, "Genetic algorithm applications for phased arrays," *Applied Computational Electromagnetics Society Journal*, vol. 21, no. 3, pp. 325-336, Nov. 2006.
- [18] X. S. Yang, *A New Metaheuristic Bat-Inspired Algorithm*. In: J. R. Gonzalez, et al. (eds), *Nature Inspired Cooperative Strategies for Optimization (NISCO 2010)*, Springer, Berlin, pp. 65-74, 2010.
- [19] A. H. Gandomi, X. S. Yang, A. H. Alavi, and S. Talatahari, "Bat algorithm for constrained optimization tasks," *Neural Computing and Applications*, pp. 1239-1255, 2012.
- [20] X. S. Yang, "Bat algorithm for multi-objective optimization," *International Journal of Bio-Inspired Computation*, pp. 267-274, 2013.
- [21] E. BouDaher and A. Hoorfar, "Electromagnetic optimization using mixed-parameter and multi-

objective covariance matrix adaptation evolution strategy," *IEEE Trans. Antennas Propag.*, vol. 63, no. 4, pp. 1712-1724, Apr. 2015.

- [22] N. Jin and Y. Rahmat-Samii, "A particle swarm optimization algorithm with hybridized real and binary parameters," *ACES Conference on Optimization Techniques for Electromagnetic Applications*, 2008.



You-Feng Cheng was born in Anhui, China, in 1989. He received his B. E. degree in Electronic Information Science and Technology from the Chengdu University of Information Technology, Chengdu, China, in 2012. He is currently working toward the Ph.D.

degree in Radio Physics at the University of Electronic Science and Technology of China (UESTC), Chengdu, China. His main research interests include phased arrays, evolutionary algorithms, and reconfigurable antennas.



Wei Shao received the M. Sc. and Ph. D. degrees in Radio Physics from UESTC, Chengdu, China, in 2004 and 2006, respectively. He joined the UESTC and is now a Professor. He has been a Visiting Scholar in the Electromagnetic Communication Laboratory, Pennsylvania State University in 2010. His research interests include computational electromagnetics and antenna design.



Xiao Ding received the B.S. and M.S. degrees in Electronic Engineering, from Guilin University of Electronic Science and Technology (GUET), Guilin, China, and the Ph.D. degree in Radio Physics from University of Electronic Science and Technology of China (UESTC), Chengdu, China, in 2014. He joined the UESTC in 2014, where he is currently an Associate Professor. In 2013, he was a Visiting Scholar at the South Dakota School of Mines and Technology, SD, USA. From June 2016 to June 2017, he was a Visiting Scholar at the University of Houston, TX, USA. His research interests include reconfigurable antennas and its' applications and phased arrays.



Meng-Xia Yu received the M.Sc. degree in Electronic Engineering and Ph.D. degree in Radio Physics from UESTC, Chengdu, China, in 1997 and 2006, respectively. She joined UESTC in 1997 and is now an Associate Professor. She has been a Visiting Scholar in the University of California, San Francisco, from 2011 to 2012. Her research interests include microwave circuits and antenna design.